

Realization of a 33 GHz phononic crystal fabricated in a freestanding membrane

Drew F. Goettler, Mehmet F. Su, Charles M. Reinke, Seyedhamidreza Alaie, Patrick E. Hopkins et al.

Citation: *AIP Advances* 1, 042001 (2011); doi: 10.1063/1.3676170

View online: <http://dx.doi.org/10.1063/1.3676170>

View Table of Contents: <http://aipadvances.aip.org/resource/1/AAIDBI/v1/i4>

Published by the [American Institute of Physics](#).

Related Articles

Morphology control of nanohelix by electrospinning
Appl. Phys. Lett. 101, 263505 (2012)

High sensitivity and fast response and recovery times in a ZnO nanorod array/p-Si self-powered ultraviolet detector
Appl. Phys. Lett. 101, 261108 (2012)

Double-templated electrodeposition: Simple fabrication of micro-nano hybrid structure by electrodeposition for efficient boiling heat transfer
Appl. Phys. Lett. 101, 251909 (2012)

Ultrananocrystalline diamond nano-pillars synthesized by microwave plasma bias-enhanced nucleation and bias-enhanced growth in hydrogen-diluted methane
J. Appl. Phys. 112, 124307 (2012)

Graphene wrapped multiwalled carbon nanotubes dispersed nanofluids for heat transfer applications
J. Appl. Phys. 112, 124304 (2012)

Additional information on AIP Advances

Journal Homepage: <http://aipadvances.aip.org>

Journal Information: <http://aipadvances.aip.org/about/journal>

Top downloads: http://aipadvances.aip.org/most_downloaded

Information for Authors: <http://aipadvances.aip.org/authors>

ADVERTISEMENT



AIPAdvances

Now Indexed in Thomson Reuters Databases

Explore AIP's open access journal:

- Rapid publication
- Article-level metrics
- Post-publication rating and commenting

Realization of a 33 GHz phononic crystal fabricated in a freestanding membrane

Drew F. Goettler,¹ Mehmet F. Su,^{1,2} Charles M. Reinke,³ Seyedhamidreza Alaie,¹ Patrick E. Hopkins,⁴ Roy H. Olsson III,⁵ Ihab El-Kady,^{1,2,3} and Zayd C. Leseman¹

¹Department of Mechanical Engineering, University of New Mexico, Albuquerque, New Mexico, 87131, USA

²Department of Electrical Engineering, University of New Mexico, Albuquerque, New Mexico, 87131, USA

³Department of Photonics Microsystems Technologies, Sandia National Laboratories, Albuquerque, New Mexico, 87185, USA

⁴Department of Microscale Science and Technology, Sandia National Laboratories, Albuquerque, New Mexico, 87185, USA

⁵Department of MEMS Technologies, Sandia National Laboratories, Albuquerque, New Mexico, 87185, USA

(Received 8 November 2011; accepted 20 December 2011; published online 29 December 2011)

Phononic crystals (PnCs) are man-made structures with periodically varying material properties such as density, ρ , and elastic modulus, E . Periodic variations of the material properties with nanoscale characteristic dimensions yield PnCs that operate at frequencies above 10 GHz, allowing for the manipulation of thermal properties. In this article, a 2D simple cubic lattice PnC operating at 33 GHz is reported. The PnC is created by nanofabrication with a focused ion beam. A freestanding membrane of silicon is ion milled to create a simple cubic array of 32 nm diameter holes that are subsequently backfilled with tungsten to create inclusions at a spacing of 100 nm. Simulations are used to predict the operating frequency of the PnC. Additional modeling shows that milling a freestanding membrane has a unique characteristic; the exit via has a conical shape, or trumpet-like appearance. *Copyright 2011 Author(s). This article is distributed under a Creative Commons Attribution 3.0 Unported License.* [doi:10.1063/1.3676170]

I. INTRODUCTION

PnCs possess the ability to prohibit the propagation of elastic waves over a specific frequency range, which is based on the material properties and geometry of the PnC. Creation of the frequency band gap is primarily based on Bragg scattering between inclusions embedded in the host material of the PnC. Thus, the location of the band gap in the frequency domain is dependent on the lattice constant between inclusions.¹ The inclusions are typically cylindrical in shape and are filled with a fluid²⁻⁴ or a solid.⁵⁻⁷ Recent work shows that solid inclusions open wider band gaps than fluid inclusions in PnCs for a large range of frequencies.¹ Choosing the proper matrix and inclusion materials is also based on acoustic impedance, Z ($Z = \sqrt{E\rho}$), where E is the elastic modulus of the material and ρ is the density; larger differences in Z lead to wider band gaps.^{8,9} Based on these design criteria, the PnC fabricated in this work is a solid-solid PnC on a square lattice comprised of a Si host material and W inclusions.

Since PnCs can alter the wave propagation of elastic waves, phonon manipulation is possible. Considerable amounts of thermal energy are carried by phonons having frequencies above 10 GHz.¹⁰ However, the Debye model predicts that the $3k_B T$ phonons ($\hbar\omega \approx 3k_B T$), where k_B is the Boltzmann constant, T is the temperature (in Kelvin), \hbar is Planck's constant divided by 2π , and ω is the phonon frequency, contribute the most to the total energy and thus for room temperature the dominant



phonons exist around 1 THz.¹¹ In order to attain PnCs that manipulate THz frequencies, lattice constants on the order of a nanometer are necessary.¹

The highest operating frequencies reported for PnCs are in the 1-12 GHz range.^{3,7,12,13} For PnCs with 1D lattices, measurements have been made up to 12 GHz.¹³ Though appealing due to their simplicity, 1D lattices are not capable of opening band gaps nearly as wide as 2D lattices due to their decreased symmetry. For 2D lattices, frequencies up to approximately 1 GHz have been demonstrated.^{3,7} The lattice constants for the 2D PnCs were between 1.36 μm and 2.5 μm . Manipulation of THz frequency phonons requires a further reduction of the lattice constant of the inclusions and their radii. In this article, a PnC with a 2D lattice is reported that operates above 10 GHz. Its primary band gap frequency is 33 GHz with a secondary band gap at 47.5 GHz. It was fabricated in a freestanding Si membrane with W inclusions whose lattice spacing is 100 nm. The ultimate goal is to achieve a PnC with an operating frequency at 1 THz, and creating a PnC with a band gap at 33 GHz is the first step towards that goal.

II. MODELING OF BANDGAP

A two-dimensional numerical simulation of elastic waves propagating through the PnC was performed using the Finite Difference Time Domain (FDTD) method. A detailed description of the FDTD method can be found in Ref. 14. A wideband longitudinal displacement pulse is generated at one end of the PnC, and a single point detector on the other end of the PnC collects the time dependent displacement response of the crystal. The FDTD grid in the longitudinal direction (direction of propagation) is terminated by Mur absorbing boundary conditions, which prevent spurious reflections of the propagating wave at numerical grid boundaries. For the other two directions periodic boundary conditions are implemented, effectively creating a structure of infinite extent in those directions. The Fast Fourier Transform (FFT) technique is utilized to recover the frequency domain response from the collected time domain displacement data. Figure 1 (bottom) shows the band gap predicted by the FDTD simulation of the 2D PnC fabricated for this article.

The simulation uses W inclusions in a simple cubic lattice with a radius of 16 nm spaced 100 nm apart within a Si matrix. In the simulations W was given a density of 19.25 g/cm³, a longitudinal sound velocity of 4611 m/s, and a transverse sound velocity of 2890 m/s. Si had a density of 2.33 g/cm³, 8520 m/s for a longitudinal sound velocity, and a transverse sound velocity of 5387 m/s. Each direction in numerical space used 50 nodes per unit length, where the unit length is equal to the lattice constant. Using these parameters, a primary band gap centered at 33 GHz with a width of 14.7 GHz is predicted for this PnC along with a narrower secondary band gap centered at 47.5 GHz. Additionally, the dispersion of the Si-W PnC was calculated for the same parameters using the plane-wave expansion (PWE) technique,¹⁵ as shown in Figure 1 (top). Only the Γ -X direction in frequency space was considered to match the FDTD simulation, which excited elastic waves on one side of the PnC and detected them on the opposite parallel face. Also, the FDTD simulation excited and detected only longitudinal waves to model the effect of most transducer designs, which predominately couple to longitudinal elastic waves.¹⁶ Thus, the in-plane and out-of-plane transverse modes in Figure 1 (top) were not considered in comparing with the band gap shown in Figure 1 (bottom). Given these assumptions, the primary and secondary band gaps predicted by PWE are in excellent agreement with those predicted by FDTD; compare the shaded regions of Figure 1 for the FDTD and PWE results.

III. FABRICATION AND RESULTS

Successful fabrication of a PnC requires both an ordered-crystalline pattern and isolation from the surrounding material. The focused ion beam (FIB) is a tool that allows for control of a beam of Ga⁺ ions with nanometer precision – nanoFIBrication. This enables the creation of an ordered array of holes and for backfilling these holes with W. Suspension of the PnC allows for its isolation and direct observation of vias penetrating the entire thickness of the membrane prior to backfilling the holes with W. Therefore, fabrication is carried out with a FIB on a freestanding membrane of Si.

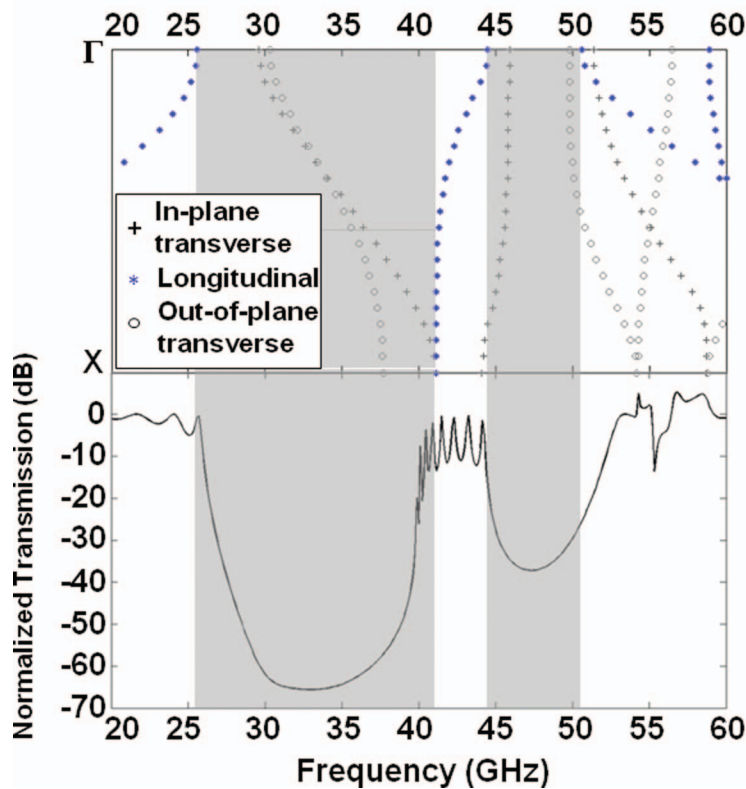


FIG. 1. Primary and secondary band gap predicted by simulations. (Bottom) Band gaps predicted by FDTD simulations for a 2D PnC with W inclusions inside a Si matrix. The inclusions have a radius of 16 nm and are spaced 100 nm apart. The primary band gap is centered at 33 GHz and has a width equal to 42% of the center frequency. (Top) Dispersion diagram in the Γ -X direction calculated with PWE showing a band gap for longitudinal modes from 26 to 41 GHz and from 45 to 50 GHz.

Figure 2 shows a square array of vias fabricated with a FIB on a freestanding Si membrane. Damage to the substrate below provides proof that the vias penetrated the entire membrane.

There are numerous models that describe via formation^{17,18} and metal deposition.¹⁹⁻²² In via formation, the incoming beam of ions is assumed to be Gaussian.^{17,23} When an ion reaches the target, it can penetrate into the sample and create a series of events that causes a particle to be ejected (or sputtered) from the surface. Depending on the size of the ion beam, lateral damage induced by the beam can be the same as or larger than the ion beam itself.²⁴ As for metal deposition, it is induced by the secondary electrons from either an electron beam or the interaction of the ion beam with the surface. In all of these explanations, it is assumed that there is only a top surface, i.e. one is milling and filling a blind hole (no exit). When milling a freestanding substrate, however, both the top and the bottom surfaces must be taken into account.

For the devices fabricated in this work, a 200 nm protective layer of Cr was deposited on the top surface of the Si. By using a protective layer, surface damage by Ga^+ ions is confined to the Cr and does not reach the surface of the thin Si membrane between each via. Cr also has the added benefit of generating better images in the SEM because of its high electrical conductivity. Upon completion of the PnC, the Cr is removed along with any sputtered material on top of the Cr.

The lower Si surface is exposed to the vacuum environment inside the vacuum chamber of the FIB, and it is 1 μm above the Si substrate. For modeling purposes, the 1 μm gap is treated as a layer of low-density N_2 . Because the lower surface is not confined by additional material below, the exiting ions and sputtered material have an additional direction to travel. This allows the ions and sputtered material to exit from both the top and bottom surface.

Using a Monte Carlo simulation package named TRIM (Transport of Ions in Matter), it can be shown that incoming ions induce damage in a cone, or trumpet shape (Figure 3(a)). TRIM

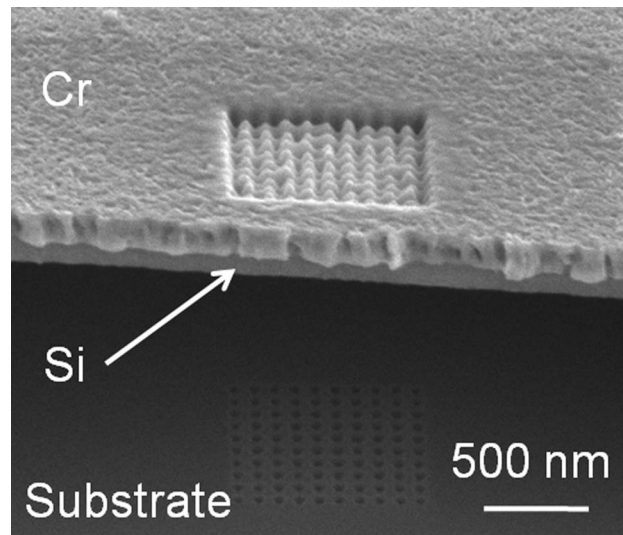


FIG. 2. SEM image of a PnC with vias spaced 100 nm apart milled into a freestanding membrane comprised of Cr, which acts as a protective layer, on top of Si. The membrane sits 1 μm above a Si substrate. Damage to the substrate below the PnC indicates complete penetration of the membrane for all 100 vias.

calculates the stopping and range of ions into matter using a quantum mechanical treatment of ion-atom collisions,²⁵ and it allows multiple layers of different materials with varying thicknesses to be modeled. The model also captures the last known position of an ion, its exit energy, and its direction cosines.

All of the TRIM modeling in this report used Ga^+ ions accelerated with a voltage of 30 kV that penetrate, beginning at a single point, a two-layer system comprised of a thin layer of Si on top of a layer of low-density N_2 . For completeness, multiple simulations were performed with various Si layer thicknesses, with the thickness ranging between 5 and 100 nm. N_2 acted as the void between the thin Si layer and the substrate. Since the focus of the TRIM modeling was to observe the shaping of the Si, Cr was not used in the model. Figure 3(a) shows a result from the TRIM modeling. A single row of ions strikes a 20 nm thick Si surface, which is on the top of Figure 3(a). On the bottom of Figure 3(a) is the low-density layer of N_2 , which is also 20 nm thick. Damage to the Si layer has a conical shape, or trumpet-like appearance, an effect that was also observed during FIB nanofabrication of the PnC (Figure 3(b)). In the TRIM model, all of the Si thickness variations predicted damage in a conical shape.

The first step in fabricating the PnCs was creating a thin device layer on a silicon-on-insulator (SOI) wafer. Studies show that thin membranes produce a band gap that is unaltered by slab modes.⁷ More specifically, the membrane must be thinner than the lattice spacing. For a 33 GHz PnC, the device layer must be less than or equal to 100 nm.

To thin the initial 450 nm thick device layer of the SOI wafer down to a thickness of 100 nm or less, thermal oxide layers were grown from the Si and subsequently etched away until the desired thickness was attained. After thinning, outlines of the PnC were patterned on the wafer. Because of the minuscule dimensions of the devices (100 nm thick and microns in width), they were prone to stiction failure.^{26–28} To minimize the possibility of stiction failure, the devices were dried using a CO_2 critical dryer.

The next step utilized the FIB to nanofabricate a square array of air holes and backfill with W. All of the FIB work was performed with FEI's Quanta 3D FEG dual beam system. The ion gun, mounted 52° from vertical, both milled the vias and then backfilled the vias with W.

A 2D square lattice of circular vias was created in the 70 nm thick freestanding Si membrane. Each circular via in the pattern was created by dwelling the ion beam at a single pixel for a set period of time rather than rastering the beam in a circular pattern around each lattice point. At each defined lattice center, the ion beam would dwell for a preset amount of time before moving to the next

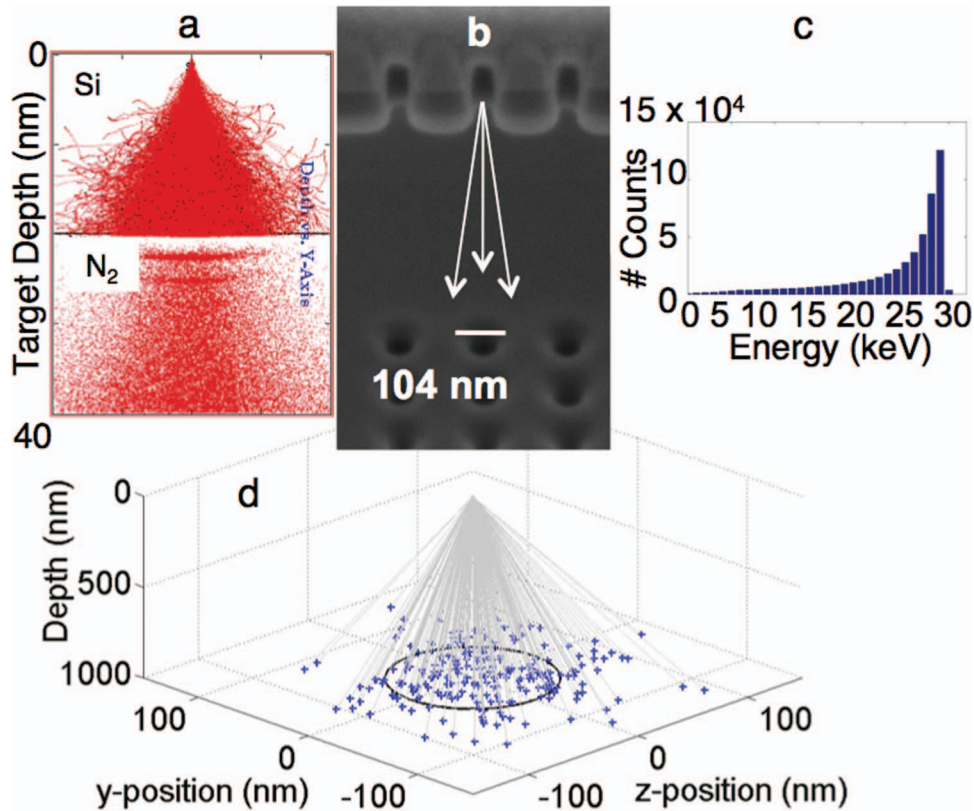


FIG. 3. Results of TRIM simulations. a) Image from TRIM showing Ga^+ ion induced damage to 20 nm thick layer of Si with N_2 gas on underside of Si. b) SEM image of a via generated in both the Si membrane and substrate. c) Distribution of Ga^+ ion energies as they exit the freestanding Si membrane. d) Results from post-processing of TRIM data. Gray lines show trajectory of Ga^+ ions ejected from the bottom of the freestanding Si surface. Blue crosses at the bottom of the y-z plane represent locations of Ga^+ ions in Si substrate. The black circle has a radius of 56.3 nm and is equal to the mean distance of the Ga^+ ions in the substrate from the x-axis (Depth).

lattice center. The voltage and current of the ion beam were set at 30 kV and 10 pA, respectively. This generated circular vias with a diameter of 32 nm. Control over the spacing between vias was determined by the pitch of the ion beam in the x and y directions, which was set to 100 nm. Setting the pitch closer eroded enough of the Cr layer to cause overlapping of the air holes in the Si layer. As the ion beam moved from one pixel to the next, the beam was not blanked (blanking the beam during milling is not allowed by the system). This meant material between the desired holes was also removed. In order to minimize this effect, the dwell time of the ion beam was maximized (25 ms) so that a minimum number of passes were made to fully penetrate the freestanding membrane. In the end, a $7 \times 7 \mu\text{m}$ array of air holes with a lattice constant of 100 nm was nanofabricated with the FIB. This generated a 71×71 air hole array, or 5041 individual vias. With such a large array and a small beam current, each pattern took approximately 40 minutes to fabricate. Because of the precision required and the amount of time needed to fabricate a single device, the die holding the membrane was mounted onto a custom 52° pre-tilt stage to minimize mechanical drift of the dual beam system. Figure 4(a) shows a completed array of vias.

After nanofabrication of the air hole array, the next step was to backfill the holes with W. The FIB system is equipped with a gas-injection system (GIS) needle that flowed tungsten hexacarbonyl gas over the device. Ray *et al.* showed that confinement of the ion beam to an area much smaller than the via during deposition (1:16 area ratio) generated vias with no voids.²⁹ To control the deposition area, a script was written to generate a pattern of circles with a specific diameter and spacing equal to the spacing between the air holes. A diameter of 8 nm provided the 1:16 area ratio. Also, the ion current had to be set to a lower value of 1.5 pA to allow a smaller area to be swept out. The

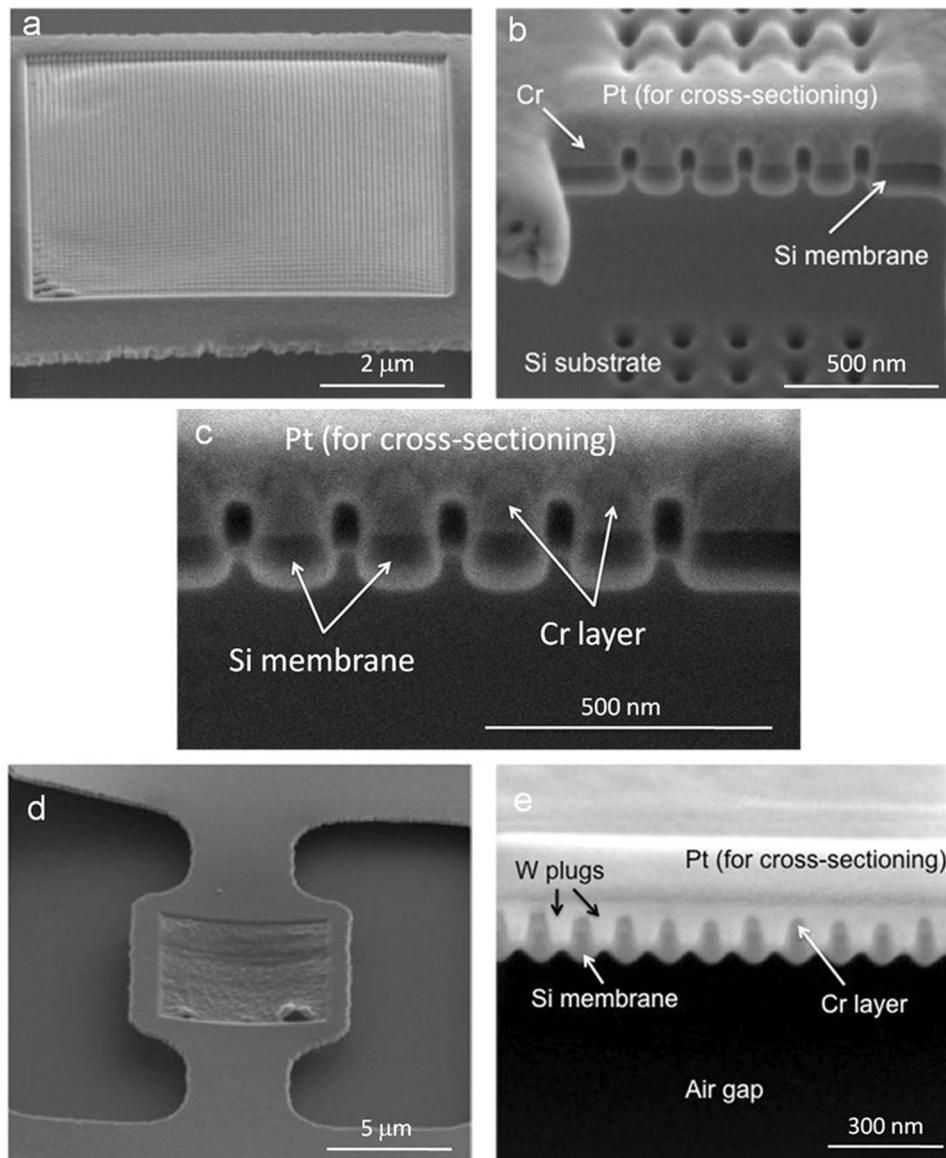


FIG. 4. SEM images of the PnC nanofabrication process with a FIB. a) $7 \times 7 \mu\text{m}$ array of vias on a freestanding membrane of Cr and Si. Hole spacing is 100 nm and each hole has a diameter of 32 nm. b) Cross-section of vias in a freestanding membrane of Cr on top of Si. A thin layer of Pt, which partially filled the vias, was placed on the Cr to preserve the shape of each via during the cross-section process. c) Close-up of vias shown in B. d) $7 \times 7 \mu\text{m}$ PnC of W inclusions in a Si membrane. e) Cross-section of W filled vias. Each via in the membrane is filled with a void-free plug of W.

accelerating voltage, however, was kept constant at 30 kV. A dwell time of 500 ns provided enough time for the W atoms to adsorb onto the sidewalls of the vias. A W-filled air hole array is shown in Figure 4(d).

A cross-section of the W-filled holes in a freestanding membrane is shown in Figure 4(e), illustrating the void-free W deposits. In Figure 4(e), the vias were covered with a layer of Pt to preserve the array during cross-sectioning.

IV. DISCUSSION

Referring to Figure 2, it is clear that a freestanding membrane allows for underside observation. Direct observation of the substrate allows confirmation of the membrane's penetration. Another

possible way to visually confirm complete penetration is by generating a cross-section of the device, but such damage to the PnC would render it useless. Variations in thickness across the wafer (± 25 nm) also prohibit one to assume that a particular z-depth setting on the FIB would work for each device.

A second observation is of the membrane's underside, which can be seen in Figure 4(b) and 4(e). Milling vias in the freestanding membrane created a *trumpet* effect as the ions exited the membrane. This result was certainly unexpected, but it can be explained by looking at the TRIM results and the molecular dynamics model by Russo.²⁴ As ions bombard the surface, they do not stay confined to the initial cross-sectional area. Instead, the ions spread out and remove material from a larger region than the incident area.

Once the ions have milled through the freestanding membrane, they continue down to the Si substrate below and can begin to mill the substrate if they have enough energy. Because the ions spread out as they leave the freestanding membrane, the via in the substrate should be bigger than the corresponding via milled into the membrane. As stated previously, TRIM captures the exit energy, position, and direction cosines of an ion. Using this energy and geometric information along with the BOX layer thickness of $1\ \mu\text{m}$, the radius of the hole in the substrate (Figure 3(b)) can be estimated.

With a 5 nm layer of Si and confining the ions to those that have energy greater than 29 keV, the mean lateral distance of the Ga^+ ions in the substrate from the x-axis is predicted to be 56.3 nm (Figure 3(d)), which is consistent with a radius of 52 nm for the holes milled in the substrate. Since the initial Ga^+ ions striking the Si sputter away the top layer and don't contribute to the lower surface being sputtered, only the last 5 nm of the Si surface is used in the TRIM model. An ion energy value of 29 keV is used since it is the mode for the statistical distribution of the transmitted ions (see Figure 3(c)).

Void-free metal deposition in a membrane via was additionally demonstrated (see Figure 4(e)). This provides evidence that metal deposition growth is initiated on the sidewalls of the vias, which agrees with the observations of Ray *et al.*, who observed accelerated deposition of metal on the sidewalls of their vias.²⁹ Due to the secondary particles (electrons and ions) generated by the ion beam's interaction with the sidewalls of the vias, metal deposition is initiated on the sidewalls. If the ion deposition beam diameter is similar to that of the via, it is more likely that metal deposition will occur only on the sidewalls, and this may create voids within the plug. By confining the ion deposition beam to an area much smaller than the via, Ray *et al.* were able to fill vias with a void-free deposition. The same approach was used here to fill vias in a freestanding membrane with similar results: void-free deposits of W.

Another interesting observation was the profiles generated by milling two different materials with different sputter rates. Compared to Si, the top layer of Cr has a higher sputter rate. Because of sputter rate differences, a non-uniform Gaussian beam profile is generated when milling stacked layers of materials with different rates (Figure 4(c)). Since the top layer of Cr has a higher sputter rate than the Si underneath, the width of the Cr hole is slightly larger than the hole in Si. Based on this, one could potentially use materials with different sputter rates to deliberately shape the beam profile in each layer.

V. CONCLUSION

Using a focused ion beam, a 2-D simple cubic PnC was nanofabricated with the FIB into a freestanding membrane of Si using a protective layer of Cr. The PnC is comprised of W plugs with a diameter of 32 nm in a simple cubic lattice, and the spacing between each inclusion is 100 nm. FDTD simulations and PWE calculations predict the PnC to have a band gap centered at 33 GHz and a width equal to 42% of the center frequency. Currently direct measurement of the bandgap is difficult since there are no transducers that operate at such a high frequency. One option, however, is to use Brillouin light scattering to characterize the PnC. Since the goal is to minimize heat transfer across the PnC, another option is to not measure the band gap and instead measure its thermal conductivity to determine its ability to minimize heat transfer. Using a Monte Carlo simulation package called TRIM, the geometry of the vias was predicted as fabricated in a freestanding membrane. Nanofabrication of a PnC in a freestanding membrane with a FIB revealed a number of interesting observations. 1)

Complete penetration of the membrane was observed. 2) Milling vias in the freestanding membrane created a “trumpet” effect as the ions exited the membrane. 3) Void-free W plugs can be fabricated in a freestanding membrane. 4) A non-uniform Gaussian beam profile is generated when milling stacked layers of material with different sputter rates.

ACKNOWLEDGMENT

DFG, MFS, SA, and ZCL would like to thank the Office of Basic Energy Sciences, Division of Materials Sciences and Engineering under Contract No. DE - FG02 - 10ER46720 (Drs. Kortan and Fitzsimmons), and the National Science Foundation under Grant No. CMMI 1056077 (Dr. Eduardo Misawa). This work was also supported by the Laboratory Directed Research and Development program at Sandia National Laboratories. Sandia National Laboratories is a multiprogram laboratory operated by the Sandia Corporation, Lockheed Martin Company, for the United States Department of Energy’s National Nuclear Security Administration under Contract No. DE-AC04-94AL85000. Portions of the work were carried out in UNM’s Manufacturing Training and Technology Center and UNM’s Nano Synthesis Facility.

- ¹ R. H. Olsson, I. El-Kady. *Meas. Sci. Technol.* **20**, 012002-012001 (2008).
- ² S. Benchabane, A. Khelif, J. Y. Rauch, L. Robert, V. Laude. *Phys. Rev. E* **73**, 065601-065601 (2006).
- ³ T. Gorishnyy, C. K. Ullal, M. Maldovan, G. Fytas, E. L. Thomas. *Phys. Rev. Lett.* **94**, 115501-115501 (2005).
- ⁴ T.-T. Wu, L.-C. Wu, Z.-G. Huang. *J. Appl. Phys.* **97**, 094916-094911 (2005).
- ⁵ I. El-Kady, R. H. Olsson, J. G. Fleming. *Appl. Phys. Lett.* **92**, 233504-233501(2008).
- ⁶ R. H. Olsson, S. X. Griego, I. El-Kady, M. Su, Y. Soliman, D. Goettler, Z. Leseman. In *IEEE International Ultrasonics Symposium*. Roma, Italy, 2009.
- ⁷ M. F. Su, R. H. Olsson, Z. C. Leseman, I. El-Kady. *Appl. Phys. Lett.* **96**, 053111-053111 (2010).
- ⁸ R. H. Olsson, J. G. Fleming, I. F. El-Kady, M. R. Tuck, F. B. McCormick. In *Transducers and EuroSensors*, 2007.
- ⁹ M. M. Sigalas, E. N. Economou. *J. Appl. Phys.* **75**, 2845 (1994).
- ¹⁰ J. P. Wolfe. *Imaging Phonons*, Cambridge University Press, 1998.
- ¹¹ L. F. Lou. *Introduction to Phonons and Electrons*, World Scientific, 2003.
- ¹² W. Cheng, J. Wang, U. Jonas, G. Fytas, N. Stefanou. *Nat. Mater.* **5**, 830 (2006).
- ¹³ N. Gomopoulos, D. Maschke, C. Y. Koh, E. L. Thomas, W. Tremel, H. J. Butt, G. Fytas. *Nano Lett.* **10**, 980-984 (2010).
- ¹⁴ M. M. Sigalas, N. Garcia. *J. Appl. Phys.* **87**, 3122-3125 (2000).
- ¹⁵ T.-T. Wu, Z.-G. Huang, S. Lin. *Phys. Rev. B* **69**, 094301-094301 (2004).
- ¹⁶ Y. M. Soliman, M. F. Su, Z. C. Leseman, C. M. Reinke, I. I. El-Kady, R. H. O. III. *Appl. Phys. Lett.* Accepted.
- ¹⁷ K. Edinger, T. Kraus. *J. Vac. Sci. Technol. B* **18**, 3190-3193 (2000).
- ¹⁸ A. A. Tseng. *J. Micromech. Microeng.* **14**, R15-R34 (2004).
- ¹⁹ R. R. Kunz, T. M. Mayer. *Appl. Phys. Lett.* **50**, 962-964 (1987).
- ²⁰ S. Lipp, L. Frey, C. Lehrer, E. Demm, S. Pauthner, H. Ryssel. *Microelectron. Reliab.* **36**, 1779-1782 (1996).
- ²¹ J. S. Ro, C. V. Thompson, J. Melngailis. *J. Vac. Sci. Technol. B*, **12**, 73-77 (1993).
- ²² X. Xu, A. D. D. Ratta, J. Sosonkina, J. Melngailis. *J. Vac. Sci. Technol. B*, **10**, 2675 (1992).
- ²³ R. Nassar, M. Vasile, W. Zhang. *J. Vac. Sci. Technol. B*, **16**:109-115 (1998).
- ²⁴ M. Russo, M. Maazouz, L. Giannuzzi, C. Chandler, M. Utlaut, B. Garrison. *Appl. Surf. Sci.* **255**, 828-830 (2008).
- ²⁵ J. F. Ziegler, J. P. Biersack, M. D. Ziegler. *SRIM The Stopping and Range of Ions in Matter*, 2008.
- ²⁶ F. W. DelRio, M. P. DeBoer, J. A. Knapp, E. D. R. Jr., P. J. Clews, M. L. Dunn. *Nature*, **4**, 629-634 (2005).
- ²⁷ D. Goettler, K. Murphy, A. Savkar, Z. Leseman. In *ASME IMECE2007*. Seattle, WA, 2007.
- ²⁸ Z. C. Leseman, S. P. Carlson, T. J. Mackin. *J. Microelectromech. Syst.* **16**, 38-43 (2007).
- ²⁹ V. Ray, N. Antoniou, N. Bassom, A. Krechmer, A. Saxonis. *J. Vac. Sci. Technol., B*, **21**, 2715-2719 (2003).